Design and optimization of a type-C tank for liquid hydrogen marine transport

Yinhua Liu [a], Peilin Zhou [a,b], Byongug Jeong [a,*], Haibin Wang [a]

[a] University of Strathclyde, Glasgow, G4 0LZ, UK
[b] Harbin Institute of Technology, China

HIGHLIGHTS

- The metal material and thickness of a large type-C liquid hydrogen tank were redesigned.
- Vapor-Cooled Shield (VCS) was firstly applied to the insulation layer of liquid hydrogen transport tanks.
- A novel model was developed for Rigid Polyurethane Foams (RPF), Self-evaporation and Forced-evaporation VCS insulations.
- SVCS and FVCS can reduce heat ingress by 34.5% and 74.55%, respectively.
- The thickness of the insulation layer can be reduced by 34.87% and 58.23% with SVCS and FVCS.

ARTICLE INFO

ABSTRACT

As one of the most promising renewable energy sources, hydrogen has the excellent environmental benefit of producing zero emissions. A key technical challenge in using hydrogen across sectors is placed on its storage technology. The storage temperature of liquid hydrogen (20 K, or −253 °C) is close to absolute zero so the storage materials and the insulation layers are subjected to extremely stringent requirements against the cryogenic behaviour of the medium. In this context, this research proposed to design a large liquid hydrogen type-C tank with AISI (American Iron and Steel Institution) type 316 L stainless steel as the metal barrier, using Vapor-Cooled Shield (VCS) and Rigid Polyurethane Foams (RPF) as the insulation layer. A parametric study on the design of the insulation layer was carried out by establishing a thermodynamic model. The effects of VCS location on heat ingress to the liquid hydrogen transport tank and insulation temperature distribution were investigated, and the optimal location of the VCS in the insulation was identified. Research outcomes finally suggest two optimal design schemes: (1) when the thickness of the insulation layer is determined, Self-evaporation Vapor-Cooled Shield (SVCS) and Forced-evaporation Vapor-Cooled Shield (FVCS) can reduce heat transfer by 47.84% and 85.86% respectively; (2) when the liquid hydrogen evaporation capacity is determined, SVCS and FVCS can reduce the thickness of the insulation layer by 50% and 67.93% respectively.

Please cite this article as: Liu Y et al., Design and optimization of a type-C tank for liquid hydrogen marine transport, International Journal of Hydrogen Energy, https://doi.org/10.1016/j.ijhydene.2023.05.102

Nomenclature

AISI	American Iron and Steel Institution
CCS	China Classification Society
FVCS	Forced-evaporation Vapor-Cooled Shield
IGC Code	International Code for the Construction
MLI	multilayer insulation
RPF	Rigid Polyurethane Foams
SVCS	Self-evaporation Vapor-Cooled Shield
VCS	Vapor-Cooled Shield
A_c	areas of the secondary barrier's long cylindrical outer surface, m^2
A_s	areas of the secondary barrier's spherical outer surface, m^2
A_{H2}	cross-sectional area of the VCS heat exchanger tube, m^2
A_{VCS}	inner wall heat exchanger area of the heat exchanger tube required for steady state heat exchanger, m^2
C	corrosion addition, mm
c_∞	specific heat of air, J/kg·K
D_c	diameter of the secondary barrier's long cylindrical outer surface, m
D_s	diameter of the secondary barrier's spherical outer surface, m
D_{VCS}	diameter of VCS heat exchanger tube, m
f	friction factor
g	acceleration of gravity, m/s^2
h	time, s
H_{in}	enthalpy of the hydrogen at the inlet of the VCS heat exchanger tube, J/kg
H_{out}	enthalpy of the hydrogen at the outlet of the VCS heat exchanger tube, J/kg
h_c	convective heat transfer coefficients of the outmost surface of the long cylinder, W/m^2·K
h_s	convective heat transfer coefficients of the outmost surface of the spherical outer surface, W/m^2·K
l	length of the RPF hollow long cylinder, m
M	maximum mass allowed to evaporate per tank per day, kg
$\dot{m}$	mass flow rate of low-temperature hydrogen gas evaporated in a cargo tank, kg/s
Nu_c	Nusselt numbers of the long cylindrical outer surface
Nu_s	Nusselt numbers of the spherical outer surface
Pr_∞	air's Prandtl number in tank surrounding
Pr_{H2}	hydrogen's Prandtl number in VCS heat exchanger tube
Q_{total}	heat transferred from the tank surrounding to the tank's outermost layer, W
Q_0	heat transfer that ingresses the liquid hydrogen inside the tank, W
Q_1	heat transfer through the RPF layer, W

Q_2	heat transfer through the Outer RPF layer, W
Q_{VCS}	heat transfer that ingresses the hydrogen gas in the VCS exchanger tubes, W
Q_{rad}	radiative heat transfer that occurs between the tank outermost surface and the tank surrounding
Q_{con}	convective heat transferred from the tank surrounding
Q_v	latent heat of vaporization of liquid hydrogen evaporation at 0.4 MPa, 20 K, J/kg
Q_c	heat conduction of the hollow long cylinder of the RPF, W
Q_s	heat conduction of spherical shell of the RPF, W
r_{R1}	radii of the cryogenic boundaries of insulation from the axis of the longitudinal axis of the tank, m
r_{R2}	radii of the hot boundaries of insulation from the axis of the longitudinal axis of the tank, m
r_{VCS}	radii of the VCS heat exchanger tube in the insulation from the axis of the longitudinal axis of the tank, K
Ra_c	air's Rayleigh number on the outer surface of a long cylinder in tank surrounding
Ra_s	air's Rayleigh number on the outer surface of a sphere in tank surrounding
Re	Reynolds number
T_1	surface temperatures of the cryogenic boundaries of the insulation, K
T_2	surface temperatures of the hot boundaries of the insulation, K
T_{VCS}	temperature of the wall of the VCS heat exchanger tube, K
T_∞	temperature of the air surrounding the tank, K
T_{in}	inlet hydrogen temperatures of the VCS heat exchanger tubes, K
T_{out}	outlet hydrogen temperatures of the VCS heat exchanger tubes, K
$\overline{T}_{H2}$	feature temperature of hydrogen in the tube, K
y	shape factor
v_∞	kinematic viscosity of air, m^2/s
v_{H2}	average velocity of the hydrogen gas in the VCS heat exchanger tube, m/s
ρ_∞	air density, kg/m^3
ρ_{H2}	density of low-temperature hydrogen gas in the VCS heat exchanger tube, kg/m^3
λ_∞	thermal conductivity of air, W/m·K
λ_R	thermal conductivity of RPF, W/m·K
β_∞	volumetric expansion coefficient of air
α_∞	thermal diffusivity of air, m^2/s
μ_{H2}	dynamic viscosity of the hydrogen gas in the VCS heat exchanger tube, Pa·s
ε	emissivity
δ	Stefan Boltzmann constant, W/m^2·K^4

Introduction

As held in Egypt in November 2022, the 27th Conference of the Parties of the UNFCCC (COP27) was focused on seeking effective ways to make consistent efforts to meet energy conservation and GHG emission reduction targets [1]. As a renewable energy source, hydrogen combustion not only has an extremely high calorific value (1.43×10^8 J/kg) - roughly three times that of gasoline (4.6×10^7 J/kg) at the same weight - but also emits no greenhouse gases or sulfides [2]. Thus, a large-scale development and utilization of hydrogen energy have been regarded as one of the most effective methods of reducing air pollution and the greenhouse effect. The European Union mandates that hydrogen energy must meet half of the European Union's basic energy demand by 2050 [3]. According to the HYDROGEN ROADMAP EUROPE report, Europe may need to generate approximately 2250 TW-hours (TWh) of hydrogen per year by 2050 [4]. In addition, hydrogen energy is highly competitive in industries such as transportation and aerospace due to its efficient energy carrier properties [5—7].

Both gaseous and liquefied hydrogen are attracting a lots of research interests, especially for storage and transport. High-pressure compressed hydrogen is the most widely used method of hydrogen storage. It boasts high hydrogen fill and release rates. However, the large tank weight and small capacity of high-pressure cylinders make it a poor choice for transporting hydrogen over long distances and on a large scale. Gaseous hydrogen can be liquefied at 1-atm pressure and 20 K ($-253\,°C$), and the density of liquid hydrogen at 1-atm pressure is approximately 800 times that gaseous hydrogen. The high energy density and the ability to transport it in large tanks make liquid hydrogen more advantageous for mass transportation [8]. However, there is a significant temperature difference between liquid hydrogen and the ambient temperature (about 280 K), which makes heat transfer through the storage tank hull and evaporation loss unavoidable [9,10]. The greatest challenging issue in liquid hydrogen transportation and storage technology is to minimize heat transfer into the cargo [11,12]. Thus, it is difficult to realize the globalization of hydrogen energy and achieve a large-scale hydrogen energy transport across different regions around the world. In this regard, hydrogen transport by ship is undoubtedly considered as an excellent choice. In 2021, the world's first hydrogen transport ship, Suiso Frontier, began operating between Japan and Australia, using vacuum insulation and panel insulation to transport 2500 m³ (No.1 & No.2 tank: 1250 m³ each) of liquid hydrogen at a time [13,14]. H. Park et al. [15] proposed a flexible vacuum membrane to aid in the vacuum insulation of medium-sized hydrogen storage tanks. A. N. Alkhaledi et al. [16] designed a liquid hydrogen carrier with four large C-tanks based on an LNG carrier, using RPF for the insulation of the tanks. During the research and development of new ships, Japanese and Australian researchers discovered that vacuum insulation is not a viable option for a large cargo containment system due to the high costs involved in the construction of large internal vacuum tanks. A new design of cargo containment system should be used. To reduce heat transfer, it was found that it would be more advantageous to replace the

vacuum and add a double insulation layer by filling the insulation layer with hydrogen to reduce heat transfer [17].

The Vapor-Cooled Shield (VCS) is a highly efficient thermal insulation device that can cool and insulate objects by using a cooling medium. It is widely used in the thermal protection of astronomical telescopes and space probes [10,18—20]. The cooling medium used by VCS for the insulation of hydrogen storage tanks is for low-temperature gaseous hydrogen, which not only has strong thermal insulation performance but also has no additional energy loss. Rigid Polyurethane Foam (RPF) is a popular thermal insulation material that provides excellent thermal insulation while also being cost-effective [21]. RPF has been used for LNG transportation [22].

In this context, this research is to investigate the effectiveness of applying RPF and VCS for a hydrogen storage system by conducting the design of a large type-C tank for ship liquid hydrogen transportation and storage. RPF, Self-evaporation Vapor-Cooled Shield (SVCS), and Forced-evaporation Vapor-Cooled Shield (FVCS) were used to create three insulation schemes. A thermodynamic model was developed and validated. The insulation layer's thermodynamic analysis was performed to investigate the effect of two VCS positions on the insulation layer's heat transfer. Finally, two tank insulation layer optimization schemes of the two type tanks were suggested in order to reduce liquid hydrogen evaporation or to reduce the thickness of the tank insulation layer.

Transportation and storage tank metal barrier design

Type-C tanks are insulated cylindrical, bi-lobe or tri-lobe shaped tanks that can be fully or partially pressurized, depending on the liquefied gas to be stored. The construction is similar to a pressure vessel, based on the cylindrical design for optimal material usage vs. internal pressure. A. N. Alkhaledi et al. [16,23] designed a large-scale hydrogen transport ship, JAMILA, which has four type-C tanks and can carry a total of 280,000 m³ of liquid hydrogen. However, there are problems of suboptimal material selection and large weight of tank shell (87,819 tonnes). In order to assess the insulation and economy of the tank, the main parameters of the MV JAMILA and the parameters of the tank are quoted. Table 1 displays the main parameters and dimensions of MV JAMILA. Table 2 displays the internal parameters of the liquid hydrogen transport tank of MV JAMILA, which have also been used in the design of this research.

Metal barrier material selection

Austenite in stainless steel is of a face-centered cubic crystal structure with superior plastic deformation ability. As the temperature decreases, the strength of austenitic stainless steel increases, while maintaining excellent plasticity and low-temperature impact resistance [24—26]. The world's first hydrogen transport ship, Suiso Frontier, has applied austenitic stainless steel as its tank material [14]. In the ocean environment where ships operate, corrosion-resistant materials are more advantageous. For example, adding Mo to 316 L

Table 1 – Main parameters and dimensions of MV JAMILA [16].

Ship parameters	Values	Units
Class	JAMILA	–
Vessel type	LH$_2$tanker	–
Total displacement	230,000	tonnes
Lightweight (LWT)	208,000	tonnes
Deadweight (DWT)	22,000	tonnes
Length overall (LOA)	370	m
Length between perpendicular (LBP)	367.5	m
Length on water line (LW)	367.9	m
Extreme breadth (B)	75	m
Depth (D)	35	m
Ship speed	18	knot
Liquid hydrogen cargo tank weight (Aluminium)	87,819 (21,955 × 4)	tonnes
Liquid hydrogen cargo tank capacity	282,400 (70,600 × 4)	m^3
Liquid hydrogen cargo weight	20,000 (5000 × 4)	tonnes
Rate of boil-off from cargo	0.1 (20 t/day)	% per day
Minimum propulsion power required for fully loaded condition	27.3	MW
Combined cycle gas & steam installed	50	MW

Table 2 – Internal parameters of the liquid hydrogen transport tank of MV JAMILA [16].

Internal tank parameters	Values	Units
Volume	70600	m^3
Diameter	26.38	m
Cylindrical section length	111.62	m
Head type	Spherical head	
Excess volume	0.252	%
Boil-off rate	0.1	%

stainless steel improves its resistance to chloride ion corrosion, making it suitable for ocean environments with high salt spray concentrations [25]. For this reason, this research has selected AISI type 316 L stainless steel as the main material for the metal barrier and an annealing process is used to eliminate excess stress. Table 3 shows the specific parameters of AISI type 316 L stainless steel.

Table 3 – AISI type 316 L stainless steel (annealed plate) related parameters [27].

Parameter names	Values	Units
Density	8 × 10^3	kg/m^3
Hardness, Brinell	146	N/mm^2
Tensile Strength, Ultimate	560	MPa
Tensile Strength, Yield	235	MPa
Elongation at Break	55	%
Modulus of Elasticity	193	GPa
Charpy Impact	103	J

Metal barrier thickness calculation

For tanks with certain internal pressure, a reasonable and rigorous design of the tank wall thickness can ensure the safety of the liquid cargo without leaks, while also controlling the weight of the tank and keeping the economy in mind.

The wall thickness of Type-C tanks used for transporting cryogenic liquid cargoes can be calculated according to the specifications of the China Classification Society (CCS) and should meet with the following requirements [28].

For the thickness of the cylindrical barrier plate,

$$t \geq \frac{p_{eq}D_i}{2\sigma_m\varphi - p_{eq}} + C \qquad (1)$$

where t is the thickness of barrier, mm; p_{eq} is the internal pressure of the tank, take 0.45 MPa; D_i is the inside diameter of the tank, 26,380 mm; σ_m is the allowable membrane stress, take 131.25 N/mm^2; C is the corrosion addition, mm. Because anti-rust treatment measures will be used on the tank's corrosion-prone areas, the corrosion increment will be ignored; φ is the welded joint efficiency facto, take 0.95 here.

For thickness of spherical end plate can be expressed by the following equation,

$$t \geq \frac{p_{eq}D_i y}{2\sigma_m\varphi - 0.5p_{eq}} + C \qquad (2)$$

where, y is the shape factor, generally to be taken as 0.55 for a spherical end.

In addition to meeting the above conditions, the thickness of plates in any area is not to be less than:

$$t_{min} = 3 + \frac{D_i}{1500} \qquad (3)$$

Finally, the thickness of the primary barrier is calculated to be 47.7 mm.

The secondary barrier

In general, the IGC Code (International Code for the Construction, 1986) requires the installation of an independent secondary barrier for liquid cargo tanks with a cargo temperature of 218 K (−55 °C) under atmospheric pressure [29]. Additionally, in the event that the liquid-tight primary barrier is damaged and the liquid cargo leaks, the secondary barrier must contain the cryogenic liquid cargo for 15 days. Thus, for liquid hydrogen transported at 20 K (−253 °C), this research designs the secondary barrier using the same AISI Type 316 L stainless steel as the main barrier and with a thickness that is consistent with that of the primary barrier.

Design of tank insulation layer

Physical model of insulation layer structure

The liquid hydrogen transportation tank consists of two layers of barriers and a layer of insulation. Insulation is formed by a combination of VCS and RPF that is installed between the metal primary and secondary barriers. Fig. 1 depicts a sketch of the liquid hydrogen transport tank under design. T_{in} and T_{out} are
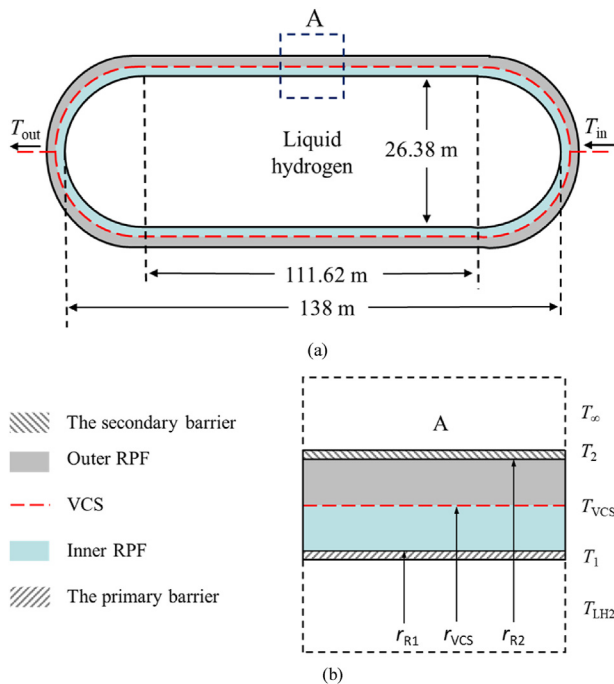
Fig. 1 – **The sketch of the liquid hydrogen transport tank under design. (a) Overall layout of the H2 tank; (b) Tank materials used between the primary and the secondary barriers.**

the inlet and outlet hydrogen temperatures of the VCS heat exchanger tubes; r_{R1} and r_{R2} are the radii of the cryogenic and hot boundaries of the insulation from the axis of the longitudinal axis of the tank; r_{VCS} is the radii of the VCS heat exchanger tube in the insulation from the axis of the longitudinal axis of the tank; T_1 and T_2 are the surface temperatures of the cryogenic and hot boundaries of the insulation; T_{VCS} is the temperature of the wall of the VCS heat exchanger tube; T_∞ is the temperature of the air surrounding the tank, 318 K;

The material of the VCS heat exchanger tubes needs to have good thermal conductivity and low temperature resistance. The VCS in this research is composed of AISI 316 L Stainless Steel heat exchanger tubes with dimensions of $\Phi 9.525$ mm × 1.245 mm. The heat exchanger tubes are spaced about 50 mm apart and arranged symmetrically around the longitudinal axis of the tank, with a total of 1460 heat exchanger tubes. All the tubes will form an insulating layer to reduce heat transfer from the outer RPF. Fig. 2 depicts the 3D schematic of how the VCS heat exchanger tubes are laid. The low-temperature hydrogen gas is through the long and thin tubes, which is approximated as a straight tube because the bending radius of the tube is much larger than the tube diameter.

Designs of insulation scheme

The design of the insulation layer for the liquid hydrogen transport tank is crucial, as it directly impacts the amount of heat transfer and evaporation of the liquid hydrogen. To reduce the amount of heat leakage and prevent excessive evaporation of the liquid hydrogen inside the tank, this thesis investigated three design schemes for the insulation layer structure of the tank as the following.
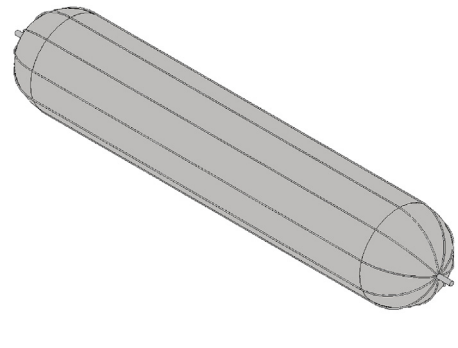

Fig. 2 – **3D schematic diagram of how the VCS heat exchanger tubes are laid.**

Single Rigid Polyurethane Foams

In this part, the insulation layer is filled with RPF. The primary method of heat transfer in the insulation layer is solid heat conduction, as shown in Fig. 3 below. Q_{total} is the heat transferred from the tank surrounding to the tank's outermost layer; Q_1 is the heat transfer through the RPF layer; Q_0 is the heat transfer that ingress the liquid hydrogen inside the tank.

Self-evaporation Vapor-Cooled Shield and Rigid Polyurethane Foams

In this part, the cryogenic hydrogen gas fed into the VCS heat exchanger tubes is self-evaporated because of external heat ingress.

As shown in Fig. 4, the heat transfer, Q_2, from the surroundings of the tank first passes through the Outer RPF by solid heat conduction. Q_2 is divided into two parts: one part of the heat transfer, Q_{VCS}, enters the low-temperature hydrogen gas and flows through the SVCS system. While the other part, Q_1, goes to the Inner RPF. Q_1 passes through the Inner RPF by solid heat conduction. The low-temperature hydrogen gas is evaporated from the liquid hydrogen due to the heat transfer Q_0.

Forced-evaporation Vapor-Cooled Shield and Rigid Polyurethane Foams

In this part, hydrogen will be used as fuel to provide energy for the operation of the ship. The fuel hydrogen is supplied from 4 liquid cargo tanks and there is no separate fuel tank. The ship is designed with a combined propulsion system of a gas turbine and a steam turbine, with a power output of 50 MW, based on the design power of the ship's operation [16]. A
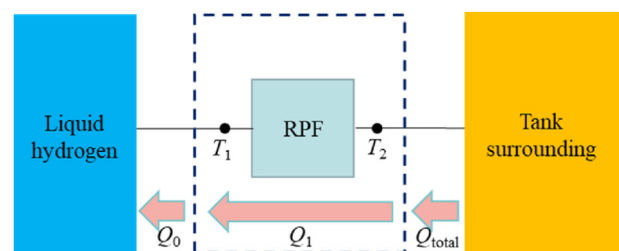

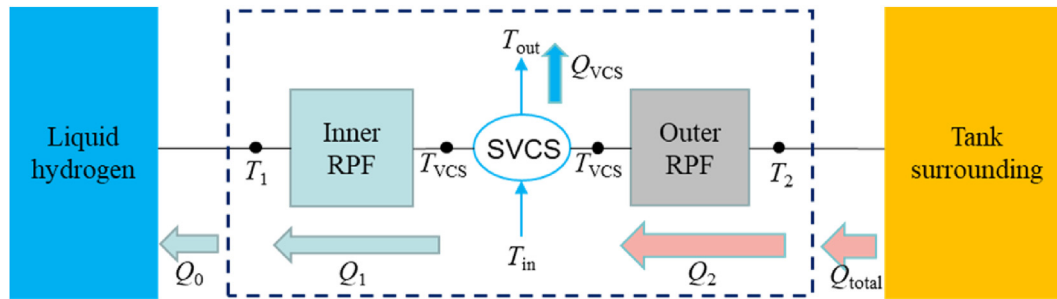Fig. 3 – **Schematic diagram of heat transfer process with single RPF.**

Fig. 4 – Schematic diagram of the heat transfer process of the insulation layer composed of SVCS and RPF.

certain amount of liquid hydrogen is extracted to the heat exchanger and forced to evaporate into cryogenic hydrogen gas. This cryogenic hydrogen gas is then fed into the VCS heat exchanger tubes to participate in the tank insulation and is finally delivered to the engine for combustion.

Fig. 5 depicts the flowchart of heat transfer diagram for FVCS. The main heat transfer processes are similar to Fig. 4, the major difference being the different mass flow rates of the cryogenic hydrogen gas fed into the VCS heat exchanger tubes.

Assumption of conditions and thermodynamic model

Assumption of conditions
This research discusses the steady-state heat exchange between the liquid hydrogen transport tank and the tank surrounding, where the evaporation of liquid hydrogen and the temperature distribution of the insulation remain constant. The following conditions are assumed:

(1) Based on the CCS Ship Design Guide, the maximum air temperature of tank surrounding is 318 K, and the maximum pressure is 0.1 MPa [28].
(2) The temperature of the liquid hydrogen in the liquid hydrogen transport tank is 20 K, and its pressure is 0.4 MPa [14]. The temperature of the primary barrier is the same as that of the liquid hydrogen; the temperature of the secondary barrier is the same as that of the outermost surface of tank.
(3) The VCS heat exchanger tubes are embedded in the RPF and in a close contact with it, and the temperature of the wall of the VCS heat exchanger tube T_{VCS} and the temperature of the RPF in contact with it are equal.

(4) All heat transferred into the liquid hydrogen transport inside the tank would contribute to boil-off gas production.
(5) Both the primary and secondary barriers are constructed using AISI type 316 L stainless steel with high thermal conductivity, resulting in negligible thermal insulation performance.

Thermodynamic model
The relevant thermodynamic model can be constructed based on the heat transfer schematic diagram.

The self-evaporation of the liquid hydrogen during ship operation is a result of heat transfer from the tank surrounding. The heat transfer between the tank surrounding and the tank's outermost layer (the secondary barrier) primarily takes place through radiation and convective of heat transfer [30].

$$Q_{total} = Q_{rad} + Q_{con} \tag{4}$$

Q_{total} is the heat transferred from the tank surrounding to the tank's outermost layer ; Q_{rad} is the radiative heat transfer that occurs between the tank outermost surface and the tank surrounding; Q_{con} is the convective heat transferred from the tank surrounding.

$$Q_{rad} = \varepsilon \delta (A_c + A_s)(T_\infty^4 - T_2^4) \tag{5}$$

in which ε is the emissivity (with a value ranging from 0 to 1). The outermost surface of the tank is protected by an aluminum-plated protective layer, and the emissivity of aluminum is 0.03; δ is the Stefan Boltzmann constant, 5.675×10^{-8} W/m^2·K^4; A_c and A_s are the areas of the secondary barrier's long cylindrical outer surface and spherical outer
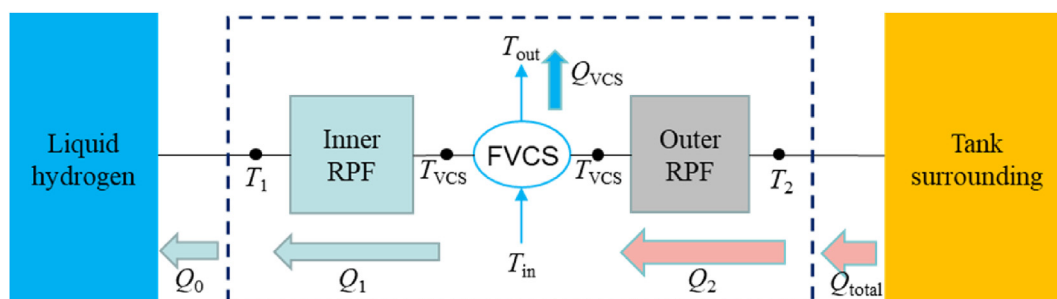

Fig. 5 – Schematic diagram of the heat transfer process of the insulation layer composed of FVCS and RPF.

surface, respectively, m²; T_∞ is the temperature of the air surrounding the tank, 318 K; T_2 is the temperature of the outermost surface of the tank, K.

$$Q_{con} = h_c A_c (T_\infty - T_2) + h_s A_s (T_\infty - T_2) \quad (6)$$

where h_c and h_s are the convective heat transfer coefficients of the outmost surface of the long cylinder and spherical outer surface, W/m²·K.

$$h_c = \frac{Nu_c \lambda_\infty}{D_c} \quad (7)$$

$$h_s = \frac{Nu_s \lambda_\infty}{D_s} \quad (8)$$

in which Nu_c and Nu_s are the Nusselt numbers of the long cylindrical outer surface and spherical outer surface; D_c and D_s are the feature sizes of the secondary barrier's long cylindrical outer surface and spherical outer surface, m; λ_∞ is the thermal conductivity of air, at a standard atmospheric pressure and 318 K, take 0.028 W/m·K.

Based on heat transfer theory [30], it is recommended that the Nussle number of the outer surface of a long cylinder be calculated using the following relation,

$$Nu_c = \left\{ 0.60 + \frac{0.387 Ra_c^{\frac{1}{6}}}{\left[1 + \left(\frac{0.559}{Pr_\infty} \right)^{\frac{9}{16}} \right]^{\frac{8}{27}}} \right\}^2 \quad (9)$$

where, Ra_c is the air's Rayleigh number on the outer surface of a long cylinder; Pr_∞ is the air's Prandtl number in tank surrounding.

$$Ra_c = \frac{g \beta_\infty D_c^3 (T_\infty - T_2)}{\alpha_\infty \nu_\infty} \quad (10)$$

where, g is the acceleration of gravity, 9.8 m/s²; β_∞ is the volumetric expansion coefficient of air, $\beta_\infty = \frac{1}{T_\infty(K)}$; ν_∞ is the. At a standard atmospheric pressure and 318 K, the kinematic viscosity of air is 1.77×10^{-5} m²/s; α_∞ is the thermal diffusivity of air, take 2.51×10^{-5} m²/s.

$$Pr_\infty = \frac{\nu_\infty}{\alpha_\infty} \quad (11)$$

$$\alpha_\infty = \frac{\lambda_\infty}{\rho_\infty c_\infty} \quad (12)$$

where, c_∞ is the specific heat of air, take 1007.41 J/kg·K; ρ_∞ is the air density, take 1.10 kg/m³.

Nusselt number on the outer surface of a sphere [30],

$$Nu_s = 2 + \frac{0.589 Ra_s^{\frac{1}{6}}}{\left[1 + \left(\frac{0.469}{Pr_\infty} \right)^{\frac{9}{16}} \right]^{\frac{4}{9}}} \quad (13)$$

Ra_s is the air's Rayleigh number on the outer surface of a sphere,

$$Ra_s = \frac{g \beta_\infty D_s^3 (T_\infty - T_2)}{\alpha_\infty \nu_\infty} \quad (14)$$

Single RPF. In the case of a single RPF, heat is transferred from the tank surrounding passes through the RPF layer and eventually to the liquid hydrogen inside the tank. The formula for this process can be expressed by using the energy conservation law,

$$Q_{total} = Q_1 = Q_0 \quad (15)$$

To ensure economy, this research requires that the boil-off rate of liquid hydrogen does not exceed 0.1% of the total mass of liquid hydrogen per day in the tank [16]. The heat to the liquid hydrogen inside the tank therefore has a requirement,

$$Q_0 \leq \frac{M * Q_v}{h} \quad (16)$$

where, M is the maximum mass allowed to evaporate per tank per day, 5,000 kg; Q_v is the latent heat of vaporization of liquid hydrogen evaporation at 0.4 MPa, 20 K, $Q_v = 4.49 \times 10^5$ J/kg; h is the time, s.

Heat conduction is the primary way of heat transfer through the RPF; convective and radiant heats are negligible.

$$Q_1 = Q_c + Q_s \quad (17)$$

where, Q_c is the heat conduction of the hollow long cylinder of the RPF, W; Q_s is the heat conduction of spherical shell of the RPF, W.

$$Q_c = \frac{2 \pi l \lambda_R (T_2 - T_1)}{\ln \left(\frac{r_{R2}}{r_{R1}} \right)} \quad (18)$$

where T_1 and T_2 are the surface temperatures on the two sides of the RPF, $T_1 = 20$ K; r_{R1} and r_{R2} are the radii of the two sides of the RPF, $r_{R1} = 13.24$ m; l is the length of the RPF hollow long cylinder, take 111.62 m; λ_R is the thermal conductivity of RPF, take 0.013 W/m·K.

$$Q_s = \frac{4 \pi \lambda_R (T_2 - T_1)}{\left(\frac{1}{r_{R1}} \right) - \left(\frac{1}{r_{R2}} \right)} \quad (19)$$

According to Eqs. (4), (15)–(17) the value of r_{R2} can be calculated, and the difference between r_{R2} and r_{R1} is the thickness of the RPF. Ultimately, the thickness of the insulation of the single RPF is calculated to be 1.84 m.

SVCS and RPF. For the insulation layer composed of Self-evaporation Vapor-Cooled Shield (SVCS) and RPF, heat transfer from the tank surrounding first passes through the outer RPF layer. When the heat transferred passes through the wall of the VCS heat exchanger tubes, the low-temperature hydrogen gas in inside the tubes absorbs some of the heat transferred. The remaining heat ingress enters to the liquid hydrogen after passing through the inner RPF layer and eventually leadings to evaporation of the liquid hydrogen. The low-temperature hydrogen gas formed by the evaporation of liquid hydrogen will then flow through along the VCS heat exchanger tubes.

In insulated systems installed with VCS, steady state heat transfer is marked by the outlet temperature of the VCS heat exchanger tube T_{out} being the same as the wall temperature of

the heat exchanger tube T_{VCS}. Once the temperature of the hydrogen in the VCS heat exchanger tube reaches the wall temperature, the hydrogen in the tube is no longer convectively heat exchanged.

$$Q_{total} = Q_2 \tag{20}$$

$$Q_1 = Q_0 \tag{21}$$

$$Q_2 = Q_1 + Q_{VCS} \tag{22}$$

The calculation of Q_2 and Q_1 are the same as Eqs. (17)–(19). Heat exchanger rate to hydrogen inside the VCS is:

$$Q_{VCS} = 1460 h_{VCS} A_{VCS}(T_{VCS} - \overline{T}_{H2}) \tag{23}$$

Where, 1460 is the number of VCS heat exchanger tubes installed in each tank; h_{VCS} is the convective heat transfer coefficient between the low-temperature gas hydrogen in the VCS heat exchanger tube and the tube wall, W/m^2·K; A_{VCS} is the inner wall heat exchanger area of the heat exchanger tube required for steady state heat exchanger, m^2; T_{VCS} is the tube wall temperature, K; $\overline{T}_{H2}$ is the feature temperature of hydrogen in the tube, K, $\overline{T}_{H2} = \frac{T_{out} - T_{in}}{2}$.

$$h_{VCS} = \frac{\lambda_{H2} Nu_{H2}}{D_{VCS}} \tag{24}$$

D_{VCS} is the diameter of VCS heat exchanger tube, take 0.007 m.

The Gnielinski correlation (25) is suitable for forced convection, including transition areas with Reynolds numbers over 3000 [30],

$$Nu_{H2} = \frac{\left(\frac{f}{8}\right)(Re - 1000)Pr_{H2}}{1 + 12.7\left(\frac{f}{8}\right)^{\frac{1}{2}}\left(Pr_{H2}^{\frac{2}{3}} - 1\right)} \tag{25}$$

where Pr_{H2} is the hydrogen's Prandtl number in VCS heat exchanger tube; f is the friction factor [30],

$$f = (0.790 \ln Re - 1.64)^{-2} \tag{26}$$

Reynolds number Re can be calculated by the following formula,

$$Re = \frac{\rho_{H2} v_{H2} L}{\mu_{H2}} \tag{27}$$

$$v_{H2} = \frac{\dot{m}}{1460 \rho_{H2} A_{H2}} \tag{28}$$

where ρ_{H2} is the density of low-temperature hydrogen gas in the VCS, kg/m^3; μ_{H2} is the dynamic viscosity of the hydrogen gas in the VCS, Pa·s; v_{H2} is the average velocity of the hydrogen gas in the VCS, m/s; A_{H2} is the cross-sectional area of the VCS heat exchanger tube, m^2; $\dot{m}$ is the mass flow rate of low-temperature hydrogen gas evaporated in a cargo tank, kg/s.

According to the law of energy conservation, the heat absorbed by VCS can also be expressed as:

$$Q_{VCS} = \dot{m}(H_{in} - H_{out}) \tag{29}$$

in which H_{in} and H_{out} are the enthalpy of the hydrogen at the inlet of the VCS tube and the enthalpy of the hydrogen at outlet of the VCS tube, J/kg.

According to assumption 4, all heat transferred to liquid hydrogen inside tank is consumed for liquid hydrogen evaporation.

$$Q_0 = Q_v \times \dot{m} \tag{30}$$

The above equations will form a closed thermodynamic model of the insulation of SVCS and RPF. As the installation position of the SVCS within the insulation varies, there will be different heat transfer and heat distribution in insulation.

FVCS and RPF. The daily hydrogen consumption of a combined propulsion system with a total power output of 50 MW is 68.9 tonnes. It means that each hydrogen transport tank's FVCS heat changer tubes need pass 17.225 tonnes of hydrogen per day [16]. Where the hydrogen consumption and the diameter of the FVCS heat exchanger tube are determined, the mass flow rate per heat exchanger tube can be determined,

$$\dot{m} = \frac{M}{h} \tag{31}$$

With the FVCS installed, the final calculation of the mass flow rate of cryogenic hydrogen gas to be forcibly evaporated per cargo tank is 0.20 kg/s.

Model validation

The conclusions of Jiang et al. [31] on the liquid hydrogen-oxygen pair storage combined with Multi-layer Insulation (MLI) and SVCS have been used to verify the thermodynamic model in this research. They installed the VCS at 50% of the MLI and used the self-evaporating hydrogen from the liquid hydrogen tank to insulate the tank. Table 4 shows the physical parameters of the model they researched. As shown in Fig. 6, the red curve represents the temperature distribution result calculated using the thermodynamic model develop in this research, while the purple stars represent the research results

Table 4 – The physical parameters of the model that Jiang et al. researched.

| Name	Parameters	Values
Tank	Shape	cylinder
	Height	3.05 m
	Diameter	3.05 m
	Head type	2:1 elliptical dome
MLI	Low density	8 layers/cm (10 layers)
	Medium density	12 layers/cm (15 layers)
	High density	16 layers/cm (20 layers)
	Total layers	45 layers
VCS	VCS shield area of LH2 tank	34.78 m^2
	VCS tube length of LH2 tank	52.19 m
	VCS shield area of LO2 tank	21.35 m^2
	VCS tube length of LO2 tank	30.04 m
	Inner diameter of the VCS tube	11.7 mm
	VCS tube wall thickness	0.5 mm
	VCS shield wall thickness	0.1 mm
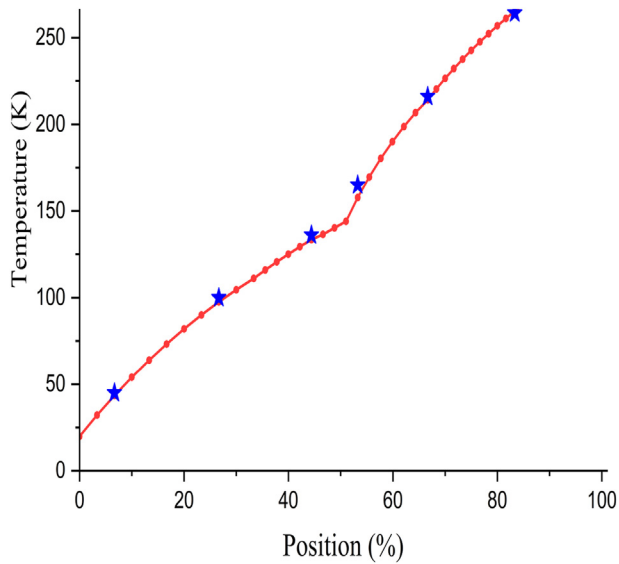
Fig. 6 – The comparison of the calculation results of the thermodynamic model in this research and the research results of Jiang et al.

of Jiang et al. The average deviation of the temperature curve inside the insulation structure is only 3.2%. It is demonstrated that the calculated value of the developed model is in consistent with the research of Jiang et al. Therefore, the model developed in this research can be applied to analyse and optimize the design of the VCS used in the insulation system of the liquid hydrogen transport tank.

Calculation results and discussion

Calculation results

The VCS is embedded within the RPF and plays a function of insulation for heat transfer from tank surrounding to the hydrogen inside the tank. The amount of heat transferred to the liquid hydrogen changes with the position of the VCS within the insulation. As for the position of the VCS, the 0% mark denotes the coldest end of the insulation that is in contact with the primary barrier, and 100% represents the hottest end of the RPF in contact with the secondary barrier.

The thickness of the RPF is taken to be 1.84 m for an insulated structure installed with VCS. This thickness is derived from the calculation of a single RPF meeting 0.1% boil-off rate of the total mass of liquid hydrogen per day in the tank.

Fig. 7 shows the relationship between the heat transferred to the liquid hydrogen and the position of the SVCS. As the installation position of SVCS moves from the primary barrier to the secondary barrier (0%→100%), the heat transferred to the liquid hydrogen decreases, then increases; the total heat transfer from the tank surrounding with the heat absorbed by the SVCS are increasing all the time.

Fig. 8 depicts the relationship between the position of the FVCS in the RPF and the heat transfer to the liquid hydrogen. The heat transfer to the liquid hydrogen decreases as the FVCS moves from the primary barrier to the secondary barrier, and
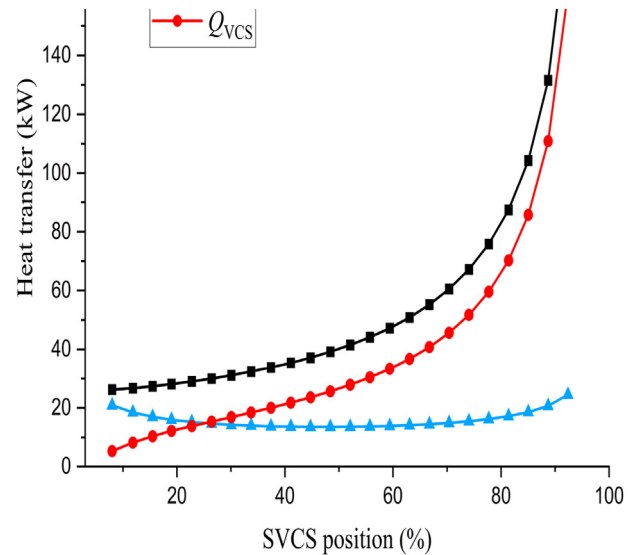

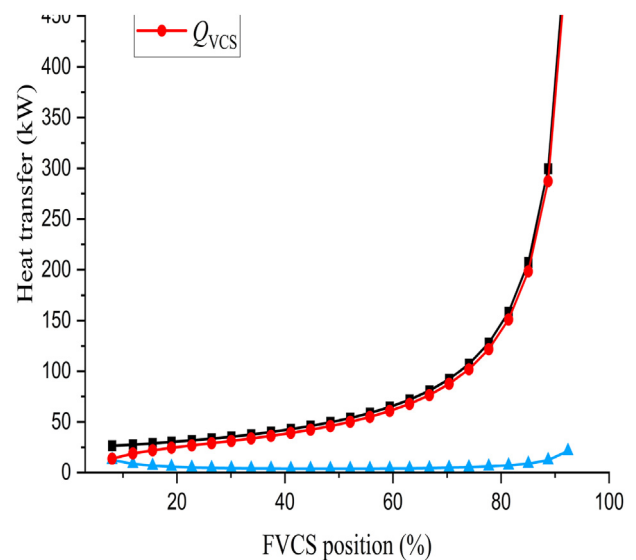**Fig. 7 – Relationship between heat transfer and SVCS position.**

Fig. 8 – Relationship between heat transfer and FVCS position.

then increases again; the total heat transfer from the tank surrounding with the heat absorbed by the FVCS are increasing all the time.

Fig. 9 depicts relationship between heat transfer Q_0 and VCS position for the three insulation structures. The single RPF has a fixed thickness and no VCS, so the heat transfer does not change. The insulation structures installed with SVCS and FVCS, both have a very strong insulation effect, and both achieve the best insulation at 50% of the insulation layer.

Fig. 10 depicts the effect of changes in the position of the VCS on the temperature of the outermost surface of the tank (T_2) and the temperature of the wall of the VCS heat exchanger tube (T_{VCS}). As the VCS moves from the primary barrier to the secondary barrier, the temperature of the outermost surface of the tank decreases, leading to an increase in heat
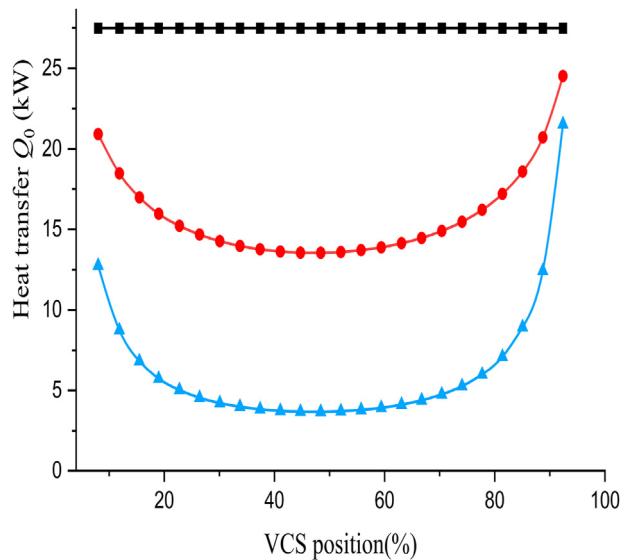
Fig. 9 — Relationship between heat transfer Q_0 and VCS position for the three insulation structures.

transferred from the tank surrounding to the liquid hydrogen transport tank. This trend aligns with the heat transfer patterns observed in Figure 7 and 8, suggesting that the position of the VCS affects heat transfer from the tank surrounding to the liquid hydrogen transport tank. Additionally, as the VCS is positioned closer to the outermost surface of the tank, the temperature of the VCS tends to increase and the temperature of the outermost surface of the tank tends to decrease, exacerbating the impact of the tank surrounding on the heat transfer of the liquid hydrogen transport tank. By comparing Fig. 10 (a) and 10 (b), it is clear that FVCS has a greater influence on the temperature of the liquid hydrogen transport tank's outermost surface. For FVCS, it can be further utilized to increase the utilization rate of low-temperature hydrogen gas.

Fig. 11 depicts the temperature profile inside the insulation layer when the SVCS and FVCS are optimally positioned. In this case, the SVCS is installed at 50% of the insulation layer, and the FVCS is installed at 50% of the insulation layer, too. Comparing the three curves, the insulation layers with VCS have significant temperature variations at the VCS installation position compared to the insulation layer with a single RPF, indicating that VCS has a significant impact on heat transfer within the insulation layer. Similarly, when comparing the SVCS and FVCS, the temperature variation of the FVCS is more pronounced, indicating that the FVCS has a greater impact on heat transfer.

Engineering practice has always expected low cost, lightweight, and simple structure implementation. In this research, two optimization design schemes for reducing the evaporation of liquid hydrogen and the thickness of the insulation layer are proposed by studying the influence of the VCS position on the heat ingress of the storage tank.

Optimization sheme 1

Fig. 9 shows the relationship between the heat transferred to the liquid hydrogen inside tank and the position of the
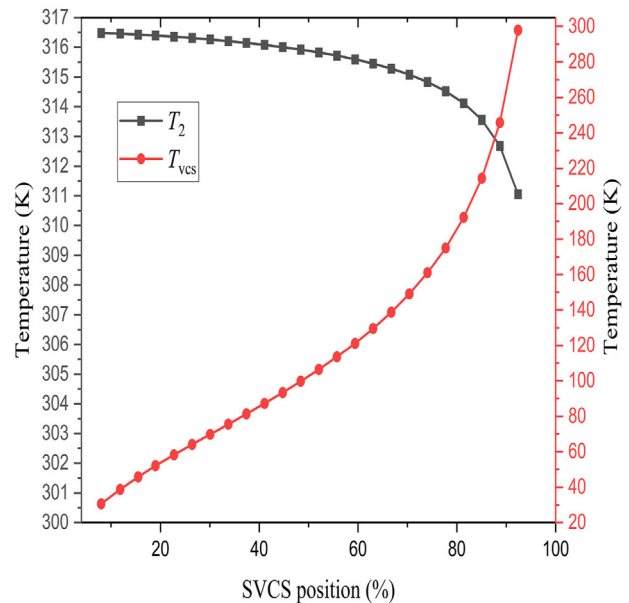
(a)
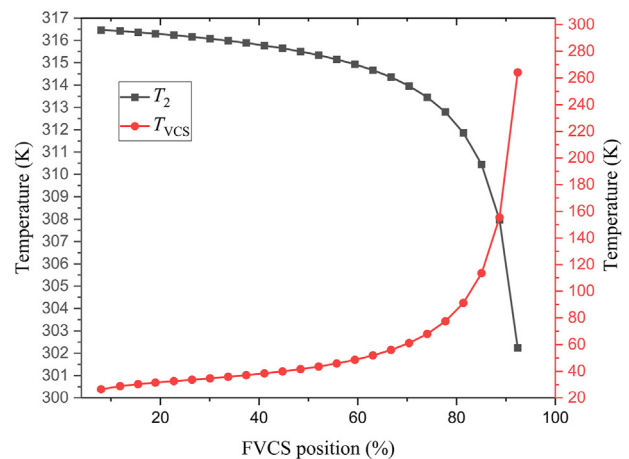
(b)

Fig. 10 — The effect of VCS position changes on T_2 and T_{VCS}. (a) SVCS position vs Temperature; (b) FVCS position vs Temperature.

VCS tubes, after the thickness has been determined to be 1.84 m.

The heat transfer of the SVCS installed at 50% of the insulation is the lowest. Relative to the boil-off rate of 0.1% of the total daily mass of liquid hydrogen in the tank, it can reduce heat transfer by 47.84% in the tank and save 2392 kg of liquid hydrogen on board per day.

The heat transfer of the FVCS installed at 50% is the lowest. Relative to the boil-off rate of 0.1% of the total daily mass of liquid hydrogen in the tank, it can reduce heat transfer by 85.86% in the tank and saving 4293 kg of liquid hydrogen on board per day.

By installing VCS at an optimal position, the loss during the transportation of liquid hydrogen can be effectively reduced.
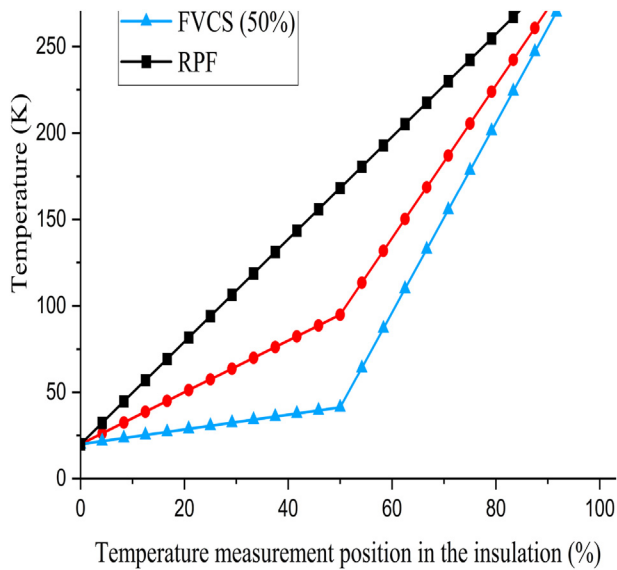
Fig. 11 — Temperature distribution inside the three insulation structures when the VCS is installed in the 50% of the insulation.
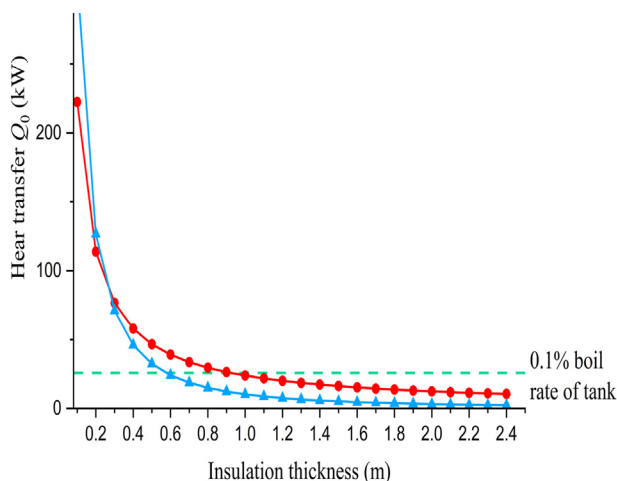

Fig. 12 — The effect of insulation thickness on the heat transfer Q_0 when the VCS is installed in the 50% of the insulation.

Optimization sheme 2

When the daily boil-off rate of liquid hydrogen is determined 0.1%, the thickness of the insulation can be reduced by installing SVCS and FVCS, it results in reduced thickness of insulation layer of RPF. Fig. 9 shows that the heat ingress is minimized when SVCS and FVCS are respectively positioned at 50% and 50% of the insulation layer. To research the impact of insulation layer thickness on heat transfer, SVCS and FVCS are installed at 50% of the insulation layer in Fig. 12.

As shown in Fig. 12, by installing SVCS, the RPF insulation layer only needs to be 0.92 m. Relative to the insulation of a single RPF with an installed thickness of 1.84 m, this scheme reduces the thickness of the insulation layer by 0.92 m (50%) compared to a single RPF insulation layer.

As shown in Fig. 12, by installing FVCS, the RPF insulation layer only needs to be 0.59 m. Relative to the insulation of a single RPF with an installed thickness of 1.84 m, this sheme reduces the thickness of the insulation layer by 1.25 m (67.93%) compared to a single RPF insulation layer.

Conclusions

This research designed a large C-tank for transporting liquid hydrogen by ships, calculated the barrier thickness, selected the barrier material and proposed three insulation strategies. The performances of the three insulation layers (single RPF, SVCS and RPF, FVCS and RPF) are investigated using a thermodynamic model, include the effect of the VCS position on heat transfer and temperature distribution in the insulation layer. Furthermore, the optimal positions of the VCS in the insulation are identified, and two different optimization schemes are proposed based on the research findings. Major conclusive remarks are presented as follows:

(1) The thickness of the primary barrier and secondary barrier are designed to be 47.70 mm, and AISI type 316 L Stainless Steel (annealed plate) is chosen as their material.

(2) Installing VCS in the insulation layer can significantly reduce heat transfer to the liquid hydrogen inside the tank. The heat transfer to the liquid hydrogen decreases and then increases as the VCS moves from the from the primary barrier to the secondary barrier (0%→100%) in the insulation layer. The optimal heat transfer position for SVCS and FVCS both are 50%.

(3) An optimized scheme for reducing liquid hydrogen evaporation loss is investigated. As stated above, when the thickness of the insulation layer remains constant, installing the SVCS at 50% of the insulation layer can reduce heat transfer by 47.84% in the tank and save 2392 kg of liquid hydrogen on board per day; installing the FVCS at 50% of the insulation layer can reduce heat transfer by 85.86% in the tank and saving 4293 kg of liquid hydrogen on board per day. This optimization scheme can significantly reduce liquid hydrogen boil-off rate during ship transportation.

(4) An optimized scheme for the thickness of the insulation layer is designed. When satisfying the boil-off rate of liquid hydrogen to be less than 0.1% per day, installing SVCS at 50% of the insulation layer can reduce the thickness of the insulation layer by 0.92 m (50%) compared to a single RPF insulation layer; installing FVCS at 50% of the insulation layer can reduce the thickness by 1.25 m (67.93%). This optimized scheme can effectively reduce transportation tank's volume and weight while also reducing construction costs.

Declaration of competing interest

The authors declare that they have no known competing financial interests or personal relationships that could have appeared to influence the work reported in this paper.

REFERENCES

[1] The 27th conference of the Parties of the UNFCCC; 2022. https://unfccc.int/event/cop-27. [Accessed 25 April 2023].

[2] Van Hoecke L, Laffineur L, Campe R, Perreault P, Verbruggen SW, Lenaerts S. Challenges in the use of hydrogen for maritime applications. Energy Environ Sci 2021;14:815–43. https://doi.org/10.1039/D0EE01545H.

[3] Fetting C. The European green deal. December: ESDN Report; 2020.

[4] Hydrogen roadmap Europe: a sustainable pathway for the European energy transition. https://www.h2knowledgecentre.com/content/researchpaper1125. [Accessed 25 April 2023].

[5] Burhan M, Shahzad MW, Oh SJ, Ng KC. A pathway for sustainable conversion of sunlight to hydrogen using proposed compact CPV system. Energy Convers Manag 2018;165:102–12. https://doi.org/10.1016/j.enconman.2018.03.027.

[6] Yılmaz İ, İlbaş M, Taştan M, Tarhan C. Investigation of hydrogen usage in aviation industry. Energy Convers Manag 2012;63:63–9. https://doi.org/10.1016/j.enconman.2011.12.032.

[7] Cau G, Cocco D, Petrollese M, Kær SK, Milan C. Energy management strategy based on short-term generation scheduling for a renewable microgrid using a hydrogen storage system. Energy Convers Manag 2014;87:820–31. https://doi.org/10.1016/j.enconman.2014.07.078.

[8] Scita R, Raimondi PP, Noussan M. Green hydrogen: the holy grail of decarbonisation? An analysis of the technical and geopolitical implications of the future hydrogen economy. https://dx.doi.org/10.2139/ssrn.3709789; 2020.

[9] Fesmire J. Research and development history of glass bubbles bulk-fill thermal insulation systems for large-scale cryogenic liquid hydrogen storage tanks. https://ntrs.nasa.gov/citations/20180006604; 2017.

[10] Zheng J, Chen L, Wang J, Zhou Y, Wang J. Thermodynamic modelling and optimization of self-evaporation vapor cooled shield for liquid hydrogen storage tank. Energy Convers Manag 2019;184:74–82. https://doi.org/10.1016/j.enconman.2018.12.053.

[11] Sinigaglia T, Lewiski F, Martins MES, Siluk JCM. Production, storage, fuel stations of hydrogen and its utilization in automotive applications-a review. Int J Hydrogen Energy 2017;42:24597–611. https://doi.org/10.1016/j.ijhydene.2017.08.063.

[12] Fesmire J, Swanger A, Jacobson J, Notardonato W. Energy efficient large-scale storage of liquid hydrogen. In: IOP conference series: materials science and engineering. IOP Publishing; 2022, 012088. https://iopscience.iop.org/article/10.1088/1757-899X/1240/1/012088/meta.

[13] Kick start for new clean energy trade. The Motorship; 2020. . [Accessed 25 April 2023].

[14] Safety requirements for carriage of liquefied hydrogen in bulk. International Maritime Organization (IMO); 2016.

[15] Park H, Kim J, Bergan PG, Chang D. Structural design of flexible vacuum insulation system for large-scale LH2 storage. Int J Hydrogen Energy 2022;47:39179–92. https://doi.org/10.1016/j.ijhydene.2022.09.063.

[16] Alkhaledi AN, Sampath S, Pilidis P. A hydrogen fuelled LH2 tanker ship design. Ships Offshore Struct 2022;17:1555–64. https://doi.org/10.1080/17445302.2021.1935626.

[17] Revision of the interim recommendations for carriage of liquefied hydrogen in bulk. International Maritime Organization (IMO); 2021.

[18] Guo Y, Lin G, He J, Bai L, Zhang H, Miao J. Experimental study on the supercritical startup and heat transport capability of a neon-charged cryogenic loop heat pipe. Energy Convers Manag 2017;134:178–87. https://doi.org/10.1016/j.enconman.2016.12.038.

[19] Dye S, Johnson W, Plachta D, Mills G, Buchanan L, Kopelove A. Design, fabrication and test of Load Bearing multilayer insulation to support a broad area cooled shield. Cryogenics 2014;64:135–40. https://doi.org/10.1016/j.cryogenics.2014.06.001.

[20] Zheng J, Chen L, Cui C, Guo J, Zhu W, Zhou Y, et al. Experimental study on composite insulation system of spray on foam insulation and variable density multilayer insulation. Appl Therm Eng 2018;130:161–8. https://doi.org/10.1016/j.applthermaleng.2017.11.050.

[21] Carriço CS, Fraga T, Carvalho VE, Pasa VM. Polyurethane foams for thermal insulation uses produced from castor oil and crude glycerol biopolyols. Molecules 2017;22:1091. https://doi.org/10.3390/molecules22071091.

[22] Kang D, Yun S, Kim B-k. Review of the liquid hydrogen storage tank and insulation system for the high-power locomotive. Energies 2022;15:4357. https://doi.org/10.3390/en15124357.

[23] Mozah. Samsung's contribution to the Q-max LNG tanker series, vol. 2008. Significant Ships of; 2008.

[24] Park WS, Yoo SW, Kim MH, Lee JM. Strain-rate effects on the mechanical behavior of the AISI 300 series of austenitic stainless steel under cryogenic environments. Mater Des 2010;31:3630–40. https://doi.org/10.1016/j.matdes.2010.02.041.

[25] Qiu Y, Yang H, Tong L, Wang L. Research progress of cryogenic materials for storage and transportation of liquid hydrogen. Metals 2021;11:1101. https://doi.org/10.3390/met11071101.

[26] Wang Z, Wang Y, Afshan S, Hjalmarsson J. A review of metallic tanks for H2 storage with a view to application in future green shipping. Int J Hydrogen Energy 2021;46:6151–79. https://doi.org/10.1016/j.ijhydene.2020.11.168.

[27] AISI type 316L stainless steel, annealed plate. https://asm.matweb.com/search/SpecificMaterial.asp?bassnum=mq316p. [Accessed 25 April 2023].

[28] Society CC. Rules for construction and equipment OF SHIPS carrying liquefied gases in bulk. 2022. p. 49–53.

[29] International Code for the construction and equipment of ships carrying liquefied gases in bulk. International Maritime Organization (IMO); 2016.

[30] Bergman TL, Lavine AS, Incropera FP, DeWitt DP. Introduction to heat transfer. John Wiley & Sons; 2011. p. 136–585.

[31] Jiang W, Zuo Z, Sun P, Li P, Huang Y. Thermal analysis of coupled vapor-cooling-shield insulation for liquid hydrogen-oxygen pair storage. Int J Hydrogen Energy 2022;47:8000–14. https://doi.org/10.1016/j.ijhydene.2021.12.103.